

Unified study of glass and jamming rheology in soft particle systems

Atsushi Ikeda,¹ Ludovic Berthier,¹ and Peter Sollich²

¹Laboratoire Charles Coulomb, UMR 5221 CNRS and Université Montpellier 2, Montpellier, France

²King's College London, Department of Mathematics, Strand, London WC2R 2LS, United Kingdom

(Dated: May 22, 2018)

We explore numerically the shear rheology of soft repulsive particles at large volume fraction. The interplay between viscous dissipation and thermal motion results in multiple rheological regimes encompassing Newtonian, shear-thinning and yield stress regimes near the ‘colloidal’ glass transition when thermal fluctuations are important, crossing over to qualitatively similar regimes near the ‘jamming’ transition when dissipation dominates. In the crossover regime, glass and jamming sectors coexist and give complex flow curves. Although glass and jamming limits are characterized by similar macroscopic flow curves, we show that they occur over distinct time and stress scales and correspond to distinct microscopic dynamics. We propose a simple rheological model describing the glass to jamming crossover in the flow curves, and discuss the experimental implications of our results.

PACS numbers: 62.20.-x, 83.60.La, 83.80.Iz

The emergence of solidity in disordered assemblies of repulsive particles is a well-known phenomenon [1] which remains difficult to understand at a fundamental level [2, 3]. When compressed, a colloidal suspension undergoes a ‘glass transition’ from (metastable) thermal equilibrium [4], as observed experimentally for a broad spectrum of particle types [5]. For colloidal hard spheres suspended in a solvent of viscosity η_s , the shear viscosity, η_T , is a universal function of the packing fraction φ , $\eta_T/\eta_s = G(\varphi)$, independently of e.g. particle size [6]. Solidity also emerges far from equilibrium upon compressing non-Brownian suspensions of repulsive particles across the ‘jamming transition’, as in foams or granular materials [3, 5]. The viscosity η_0 of a non-Brownian hard sphere suspension is again universal, $\eta_0/\eta_s = J(\varphi)$ [7]. Depending on the community and the particular system at hand, rheologists use a broad variety of functional forms and empirical models for $G(\varphi)$ and $J(\varphi)$, while underlying physical processes for both limits are often not distinguished in rheology textbooks [8]. Our aim is to determine if and how these two ideal limits are interrelated, addressing also the non-linear rheological regimes and the additional effects of particle size and softness.

Glass and jamming transitions share important similarities, in particular at the rheological level. In both cases, solidity emerges near a ‘critical’ volume fraction below which the material is a fluid whose viscosity increases rapidly with φ . The amorphous solid at large density responds elastically for small deformation, but flows when a stress larger than a yield stress is applied [1]. The dynamics becomes very heterogeneous near the critical density; its spatial correlations are usually interpreted by appealing to underlying phase transitions [9], though the nature of these remains a subject of debate [2, 3]. Based on these similarities, a unified jamming phase diagram has been proposed where thermal and athermal systems appear as a single ‘jammed’ phase [10, 11].

At the theoretical level, recent results have clarified the

relation between glass and jammed phases [12–14], suggesting that the jamming transition occurs well inside the non-ergodic glassy phase. For systems of soft repulsive particles, as studied below, a glass transition line $T_G(\varphi)$ separates the fluid (at high T , low φ) from the glass (at low T , large φ), while the jamming transition occurs upon compression at $T = 0$ inside the glass phase [14]. However, these static calculations shed little light on either dynamical properties or rheology [15]. Although this theoretical scenario appears in broad agreement with numerical work [11, 16], glass and jamming transitions are typically located using different sets of methods and observables, normally requiring extrapolation [16]. Similar ambiguities exist in experimental work where e.g. estimates for the location of the colloidal glass transition cover the range $\varphi_G \approx 0.57 \dots 0.635$, depending on how the divergence of $G(\varphi)$ is extrapolated [4, 6, 17]. In the same vein, data for the divergence of $J(\varphi)$ for athermal suspensions lie in the range $\varphi_J \approx 0.585 \dots 0.66$ [7, 16, 18].

In this paper, we argue that a clearer picture emerges when the non-linear rheology of both thermal and athermal suspensions is considered. We use computer simulations to investigate the flow properties of concentrated assemblies of soft repulsive particles, and vary the relative strength of thermal fluctuations and viscous dissipation to study the crossover from thermalized suspensions (relevant to soft colloids) to purely athermal ones (relevant to jammed solids) within a single computational framework. This setting allows us to observe and disentangle multiple rheological regimes within a single system, establishing in particular unambiguously that the increases of the shear viscosities $\eta_T(\varphi)$ and $\eta_0(\varphi)$ upon compression are unrelated. This has important consequences for the jamming phase diagram of soft particles. Although glass and jamming limits are characterized by similar macroscopic flow curves, we also show that they in fact occur over well-separated time and stress scales and correspond to qualitatively different microscopic dynamics.

We analyze theoretically the behaviour of sheared assemblies of soft repulsive particles immersed in a solvent, such as star polymers, microgels, or dense emulsions [5]. The simplest way to model these systems at large packing fraction is to ignore hydrodynamic interactions and consider only pairwise repulsion between particles, such as $V(r) = \epsilon(1 - r/a)^\alpha \Theta(a - r)$, where $\Theta(x)$ is the Heaviside function, and a is the particle diameter [19]. We use molecular dynamics simulations to study the steady state rheology of harmonic spheres, $\alpha = 2$, in a simple shear flow. We simulate the following Langevin dynamics,

$$\xi \left(\frac{\partial \vec{r}_i}{\partial t} - \dot{\gamma} y_i \vec{e}_x \right) = - \sum_{j \neq i} \frac{\partial V(|\vec{r}_i - \vec{r}_j|)}{\partial \vec{r}_i} + \vec{f}_i(t), \quad (1)$$

where \vec{r}_i and y_i represent the position and the y -coordinate of particle i , respectively, and \vec{e}_x is the unit vector along the x -axis. The damping coefficient, ξ , which accounts for viscous dissipation, and the random force \vec{f}_i describing thermal fluctuations obey the fluctuation-dissipation relation, $\langle \vec{f}_i(t) \vec{f}_j(t')^T \rangle = 2k_B T \xi \delta_{ij} \mathbf{1} \delta(t - t')$, where k_B is Boltzmann's constant.

The Langevin dynamics in Eq. (1) is characterized by two microscopic timescales: $\tau_0 = \xi a^2 / \epsilon$ controls the dissipation, while $\tau_D = \xi a^2 / (k_B T) = \tau_0 \epsilon / (k_B T)$ sets the timescale for Brownian motion. Therefore, τ_D and τ_0 are comparable at high temperatures but become well-separated when $k_B T \ll \epsilon$, with $\tau_D \gg \tau_0$. The shear rate $\dot{\gamma}$ introduces a third timescale, $\dot{\gamma}^{-1}$, from which the Péclet number is defined, $P_e = \dot{\gamma} \tau_D$. Timescale separation at low T allows us to separately explore the thermal regime at small $\dot{\gamma}$, $P_e \ll 1$, where Brownian motion is relevant, and the athermal regime at larger $\dot{\gamma}$, $P_e \gg 1$, where the suspension is non-Brownian. In the alternative SLLOD dynamics frequently used to shear suspensions [20], inertia is included and the thermostat is the only source of dissipation. Thus, the only accessible regime is $P_e < 1$ (with now $\tau_D = \sqrt{\frac{m a^2}{k_B T}}$), and the $T \rightarrow 0$ limit is unphysical. By contrast, Eq. (1) can be simulated at $T = 0$ (i.e., $P_e = \infty$), where the dynamics becomes similar to earlier studies of the jamming transition [21]. Thus, Eq. (1) allows us to study thermal and athermal systems under shear in a unified manner.

We study a 3d system of $N = 10^3$ harmonic spheres, using a 50:50 mixture of spheres with diameter ratio 1.4 to avoid crystallisation [16, 21]. We measure length in units of the small particle diameter, a , time in units of τ_0 and temperature in units of ϵ/k_B . We integrate Eq. (1) at constant $\dot{\gamma}$ using Heun's method with Lees-Edwards periodic boundary conditions [20] over a typical simulation time of at least $10/\dot{\gamma}$. We evaluate the xy -component of the shear stress, σ , using the Irving-Kirkwood formula, and deduce the shear viscosity, $\eta = \sigma/\dot{\gamma}$. The stress and viscosity units are respectively ϵ/a^3 and ξ/a . For thermal simulations at low temperatures, we combine data from Langevin and SLLOD dynamics to broaden the range

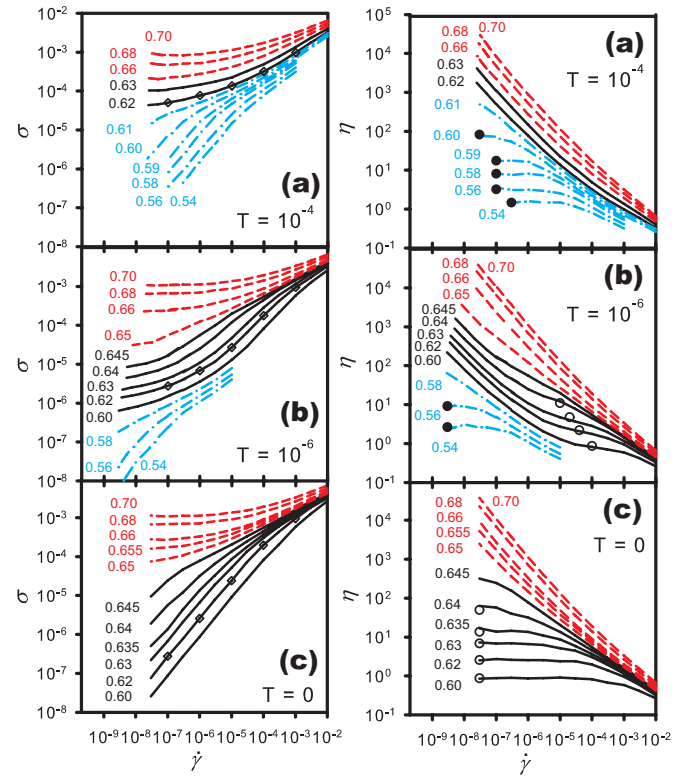


FIG. 1: Flow curves at different temperatures and densities, shown as $\sigma(\dot{\gamma})$ (left) or $\eta(\dot{\gamma})$ (right). Diamonds (left) mark the state points analyzed in Fig. 3. Circles (right) indicate thermal (closed) and athermal (open) viscosities reported in Fig. 2. Flow curves are shown in blue (dot-dashed) when thermal Newtonian behaviour is observed, in red (dashed) when thermal effects are negligible, in black otherwise.

of shear rates towards very low Péclet numbers, where SLLOD is more efficient. We have checked that both methods yield equivalent results at equal P_e values [31].

We first characterize the macroscopic flow properties at $T = 10^{-4}$. Since $\tau_D = 10^4$, the data in Fig. 1a mainly cover the thermal range, $P_e < 1$. Accordingly, the resulting flow curves are typical of dense fluids sheared across the glass transition [15, 22, 23]. Briefly, for densities $\varphi < \varphi_G \approx 0.61$, flow curves are Newtonian at low shear rates, while for larger $\dot{\gamma}$, the external flow accelerates structural relaxation leading to shear-thinning. The Newtonian viscosity, $\eta_T(\varphi)$, increases rapidly upon compression towards φ_G . Above φ_G , the linear viscosity is too large to be measured, and the system behaves instead as a solid (a glass) with a finite yield stress, defined as $\sigma_Y = \lim_{\dot{\gamma} \rightarrow 0} \sigma(\dot{\gamma})$. Both the shear viscosity $\eta_T(\varphi)$ and the yield stress $\sigma_Y(\varphi)$ can be used to locate the glass transition, which corresponds to either the divergence of η_T , or the emergence of a finite σ_Y , see Fig. 2.

At significantly lower temperature, $T = 10^{-6}$, the above phenomenology persists as long as $P_e < 1$, which now corresponds to very low shear rates, $\dot{\gamma} < \tau_D^{-1} = 10^{-6}$ in Fig. 1b. Thus, we can determine a Newtonian viscosity

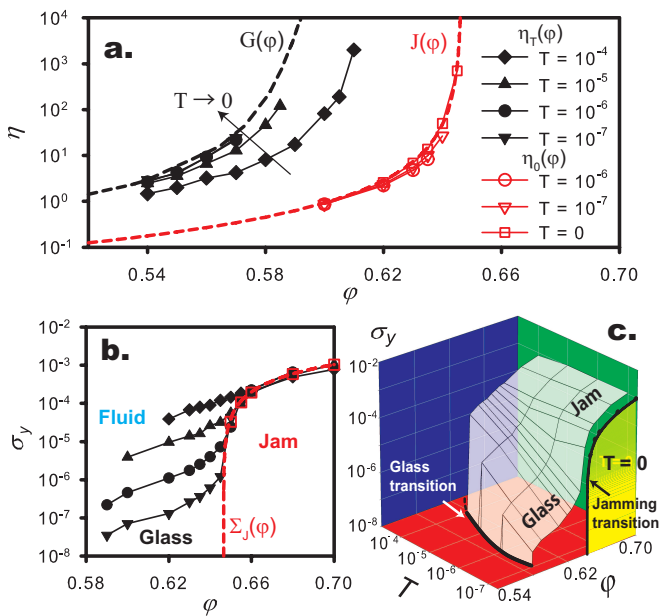


FIG. 2: (a) Shear viscosities η_T and η_0 and their distinct hard sphere limits $G(\phi)$ [17] and $J(\phi)$ [21]. (b) Density dependence of yield stress for different temperatures, including the $T = 0$ limit. (c) Same data as in (b) in a ‘glass-jamming phase diagram’.

$\eta_T(\phi)$ for $\dot{\gamma} \rightarrow 0$ and $\phi < \phi_G \approx 0.59$, and a finite yield stress above ϕ_G . Note that ϕ_G decreases slowly with decreasing T , see Ref. [16]. Because τ_D is very large, there now exists a broad $\dot{\gamma}$ window where $P_e \gg 1$ and thermal fluctuations play little role. Surprisingly, the data in Fig. 1b show that for a range of densities *above* the glass transition, $0.59 < \phi < 0.63$, the system flows as a simple Newtonian fluid when $P_e \gg 1$. This allows us to define a second viscosity, η_0 , that grows upon compression towards $\phi_J \approx 0.64$. Finally, for $\phi > \phi_J$, the flow curves are mainly characterized by a yield stress, $\sigma_Y(\phi)$. The shear viscosities $\eta_T(\phi)$ and $\eta_0(\phi)$ (Fig. 2a) obey clearly distinct behaviours. While the growth of η_T reflects the approach to the glass transition, $\phi_G \approx 0.59$, the increase in η_0 is separately controlled by the jamming transition, $\phi_J \approx 0.64$. Given that both viscosities are defined over distinct density and shear rate regimes, and can be simultaneously observed at this temperature, it is clear that they reflect distinct phenomena, even without extrapolation to locate ϕ_G and ϕ_J more precisely. Correspondingly, the evolution of $\sigma_Y(\phi)$ in Fig. 2b is influenced by both transitions, since solidity emerges near ϕ_G , but σ_Y increases significantly near $\phi_J > \phi_G$. This is consistent with the idea that jamming mainly affects the very low temperature properties of the glass phase [14].

Finally, the rheology at $T = 0$ corresponds to $P_e = \infty$, and so the glass physics cannot operate. Despite this complete change of regime, the corresponding flow curves shown in Fig. 1c appear qualitatively very similar to the

ones obtained at $T = 10^{-4}$ in Fig. 1a. They are characterized by a Newtonian viscosity η_0 at small $\dot{\gamma}$ and low density, $\phi < \phi_J \approx 0.64$, while a yield stress emerges upon compression, $\phi > \phi_J$. These data are fully equivalent to previous rheological studies of the athermal jamming transition [21], and indeed near that transition can be collapsed using the same critical scaling. The qualitative similarity between flow curves in Figs. 1a and 1c has created confusion in the literature [15], where data obtained for systems undergoing the glass transition have been incorrectly analyzed in the athermal scenario of [21].

The shear viscosities η_T and η_0 are measured over $\dot{\gamma}$ windows that become well-separated at low T and Fig. 2a emphasizes that the difference between the two functions increases as T decreases, ruling out a smooth convergence of η_T to η_0 for $T \rightarrow 0$. Instead, we find that as $T \rightarrow 0$, $\eta_T(\phi)$ follows the same density dependence as the equilibrium relaxation time of the corresponding hard sphere fluid [17], while η_0 is well described by an algebraic divergence [18]. Our results establish that the functions $G(\phi)$ and $J(\phi)$ controlling Newtonian flow in the hard sphere limit are conceptually and quantitatively distinct.

The yield stress is another highly sensitive indicator of the differences between glass and jamming transitions, see Fig. 2b. At finite T , solid behaviour emerges near $\phi_G \approx 0.59 \dots 0.61$, which agrees with equilibrium dynamics studies [16]. The yield stress then increases smoothly with ϕ up to $\phi_J \approx 0.64$ where its density dependence changes dramatically. Also, while σ_Y scales with T below ϕ_J , it is of order unity (in our units of ϵ/a^3) above, with only a weak T -dependence scaling approximately as $\sim (\phi - \phi_J)$. Consistent with this picture, more detailed analysis shows that $\sigma_Y(\phi, T)$ follows scaling behaviour near ϕ_J very similar to the one derived in Ref. [24] for the pressure [32]. Thus glass and jammed states, having distinct physical origins, also display distinct stress scales, and remain well-separated even as $T \rightarrow 0$ in the ‘glass-jamming phase diagram’ shown in Fig. 2c. Note also that while the glass transition occurs at finite T in the unsheared system, the jamming transition exists at $T = 0$ only, so that these two limits never coexist.

The complex flow curves shown in Fig. 1 can be modelled by assuming that the stress is an additive combination, $\sigma(\dot{\gamma}) = \sigma_G + \sigma_J + \eta_s \dot{\gamma}$, of contributions from glass and jamming physics, and from the solvent. The simplest model for the glass contribution incorporating the appropriate time and stress scales is

$$\frac{\sigma_G}{(k_B T/a^3)} = \frac{\tilde{\Sigma}_G(\phi)}{[1 + (\dot{\gamma}\tau_D)^\beta]^{-1} + [\dot{\gamma}\tau_D\tilde{\tau}_G(\phi)]^{-1}}, \quad (2)$$

with the dimensionless stress $\tilde{\Sigma}_G(\phi) = \text{const.} + (\phi - \phi_G)^\alpha (\phi_J - \phi)^{-\delta} \Theta(\phi - \phi_G) \Theta(\phi_J - \phi)$, and a dimensionless timescale, $\tilde{\tau}_G(\phi)$, diverging at ϕ_G , e.g. as $\tilde{\tau}_G(\phi) \sim (\phi_G - \phi)^{-\gamma}$. In this model, the viscosity diverges at ϕ_G , $\eta_T/\eta_s \propto \tilde{\tau}_G(\phi)$ (with $\eta_s = \xi/a$), and a finite yield stress

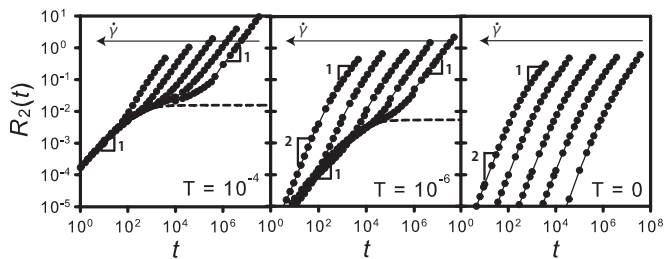


FIG. 3: Mean-square displacement at $\varphi = 0.62$ and $\dot{\gamma} = 10^{-3} \dots 10^{-7}$ and different temperatures. Caged dynamics (dashed) is only observed at finite T and $P_e \ll 1$.

emerges above, $\sigma_Y(\varphi \geq \varphi_G) = (k_B T/a^3) \tilde{\Sigma}_G(\varphi)$ which diverges near φ_J . For the jamming contribution, we use a model consistent with the scaling discussed in [21],

$$\sigma_J/(\epsilon/a^3) = \tilde{\Sigma}_J(\varphi) + [(\dot{\gamma}\tau_0)^{-\beta'} + (\dot{\gamma}\tau_0 J(\varphi))^{-1}]^{-1}, \quad (3)$$

where we take $\tilde{\Sigma}_J(\varphi) \sim (\varphi - \varphi_J)^{\alpha'} \Theta(\varphi - \varphi_J)$ and $J(\varphi) \sim (\varphi_J - \varphi)^{-\gamma'}$. The entire set of data shown in Fig. 1 can be reproduced nearly quantitatively using exponents consistent with existing results: $\alpha = 0.7$ [25], $\beta = 0.3$ [23], $\delta = 0.8$ [24], $\gamma = 2.2$ [16], $\beta' = 0.4$, $\alpha' = 1.2$ and $\gamma' = 2.0$ [21]. Our empirical model, Eqs. (2, 3), emphasizes that glass and jamming physics take place over distinct time and stress sectors, and can be addressed by independent theoretical means. Differing predictions for, e.g., whether the onset of yield stress [15, 26] is continuous, as in theories of driven athermal systems [27, 28], or discontinuous as for driven glasses [25] then make physical sense.

The distinct nature of thermal and athermal regimes is apparent also in microscopic dynamic correlation functions. We plot the mean-squared displacements, $R_2(t) = \langle |\vec{r}_i(t) - \vec{r}_i(0)|^2 \rangle$ in Fig. 3 for fixed $\varphi = 0.62$ and different T and $\dot{\gamma}$. In the glass regime, $T = 10^{-4}$, $R_2(t)$ displays short-time diffusion, caged dynamics at intermediate times, and shear driven diffusion at long times [22, 23]. At $T = 0$, we obtain very different, superdiffusive and diffusive, behaviours, as discussed in Ref. [29]. For intermediate temperature, $T = 10^{-6}$, Fig. 3 shows a clear crossover between thermal and athermal regimes: while caged dynamics is observed for low P_e , superdiffusive motion is obtained at large P_e . Therefore, the thermal-athermal crossover observed in the macroscopic rheology in Fig. 1 originates from a similar crossover at the microscopic level. While macroscopic flow curves in Fig. 1a-c can easily be confused, microscopic observations as in Fig. 3 provide a clear qualitative distinction.

We have used temperature to study the crossover between two limits, while experimentalists might equivalently tune particle softness. We note from Figs. 1a and 2b that for temperatures above $T \sim 10^{-5}$, corresponding to thermal particle compressions $(1 - r/a) \sim T^{1/2}$ of only $10^{-3} \dots 10^{-2}$, the $T = 0$ physics has little influ-

ence on the rheological behaviour. This suggests that the jamming transition cannot be studied using soft colloids unless T/ϵ is extremely small. A second relevant experimental parameter is the particle size setting the timescale for Brownian motion, with $\tau_D \sim 1$ s for particles of $1\mu\text{m}$. This implies that the present thermal-athermal crossover should be observable in experiments by tuning the particle size in the range $1\text{-}10\mu\text{m}$. Yield stress data for emulsions [30] seem consistent with the data shown in Fig. 2b, but further studies are needed to confirm our predictions.

In conclusion, we have used shear rheology to study the relationship between glass and jamming transitions. While both correspond to the emergence of solid behaviour as signalled by a finite yield stress, we have demonstrated that they occur over stress and time windows that become well-separated at low temperatures in dense repulsive systems. The glass-jamming phase diagram (Fig. 2c) has a scale-separated ‘wing’ between φ_G and φ_J , so that the glass transition line does not extrapolate to the jamming point for $T \rightarrow 0$. The two transitions can only be observed separately in these two distinct limits, i.e. on the glass line and at the jamming point. Any other state point in the phase diagram is in principle affected by a combination of both phenomena, in a way described by the simple theoretical model of Eqs. (2, 3). This conceptual clarification should help rationalize both experimental data and the scope of different theoretical approaches.

We thank M. Pica Ciamarra for discussions, and Région Languedoc-Roussillon for financial support (A.I., L.B.).

-
- [1] P. Coussot, *Rheometry of Pastes, Suspensions, and Granular Materials* (Wiley, New York, 2005).
 - [2] L. Berthier and G. Biroli, *Rev. Mod. Phys.* **83**, 587 (2011).
 - [3] A. J. Liu and S. R. Nagel, *Annual Reviews of Cond. Mat. Phys.* **1**, 347 (2010).
 - [4] P. N. Pusey and W. van Meegen, *Nature (London)* **320**, 340 (1986).
 - [5] D. T. N. Chen, Q. Wen, P. A. Janmey, J. C. Crocker, and A. G. Yodh, *Annual Review of Condensed Matter Physics* **1**, 301 (2010).
 - [6] Z. Cheng, J. Zhu, P. M. Chaikin, S. E. Phan, and W. B. Russel, *Phys. Rev. E* **65**, 041405 (2002).
 - [7] C. Bonnoit, T. Darnige, E. Clement, and A. Lindner, *J. Rheol.* **54**, 65 (2010).
 - [8] R. G. Larson, *The Structure and Rheology of Complex Fluids* (Oxford University Press, New York, 1999).
 - [9] *Dynamical heterogeneities in glasses, colloids and granular materials*, Eds.: L. Berthier, G. Biroli, J.-P. Bouchaud, L. Cipelletti, and W. van Saarloos (Oxford University Press, Oxford, 2011).
 - [10] A. J. Liu and S. R. Nagel, *Nature* **396**, 21 (1998).
 - [11] M. Pica Ciamarra, M. Nicodemi and A. Coniglio, *Soft Matter* **6**, 2871 (2010).

- [12] F. Krzakala and J. Kurchan, Phys. Rev. E **76**, 021122 (2007).
- [13] G. Parisi and F. Zamponi, Rev. Mod. Phys. **82**, 789 (2010).
- [14] H. Jacquin, L. Berthier, and F. Zamponi, Phys. Rev. Lett. **106**, 135702 (2011).
- [15] T. Voigtmann, Eur. Phys. J. E **34**, 106 (2011).
- [16] L. Berthier and T. A. Witten, EPL **86**, 10001 (2009); Phys. Rev. E **80**, 021502 (2009).
- [17] G. Brambilla, D. El Masri, M. Pierno, L. Berthier, L. Cipelletti, G. Petekidis, and A. B. Schofield, Phys. Rev. Lett. **102**, 085703 (2009).
- [18] F. Boyer, E. Guazzelli, and O. Pouliquen, Phys. Rev. Lett. **107**, 188301 (2011).
- [19] D. J. Durian, Phys. Rev. Lett. **75**, 4780 (1995).
- [20] M. Allen and D. Tildesley, *Computer Simulation of Liquids* (Oxford University Press, Oxford, 1987).
- [21] P. Olsson and S. Teitel, Phys. Rev. Lett. **99**, 178001 (2007).
- [22] R. Yamamoto and A. Onuki, Phys. Rev. E **58**, 3515 (1998).
- [23] L. Berthier and J.-L. Barrat, J. Chem. Phys. **116**, 6228 (2002).
- [24] L. Berthier, H. Jacquin, and F. Zamponi, Phys. Rev. E **84**, 051103 (2011).
- [25] M. Fuchs and M. E. Cates, Phys. Rev. Lett. **89**, 248304 (2003).
- [26] L. Berthier, J. Phys.: Condens. Matter **15**, S933 (2003).
- [27] P. Sollich, F. Lequeux, P. Hébraud, and M. E. Cates, Phys. Rev. Lett. **78**, 2020 (1997).
- [28] P. Hébraud and F. Lequeux, Phys. Rev. Lett. **81**, 2934 (1998).
- [29] C. Heussinger, L. Berthier, and J.-L. Barrat, EPL **90**, 20005 (2010).
- [30] T. G. Mason, J. Bibette, D. A. Weitz, J. Colloid Interface Sci **179**, 439 (1996).
- [31] Some simulations at very low φ and large $\dot{\gamma}$ yield configurations with ordering along the shear flow. We discard those state points.
- [32] While shear stress and pressure closely match each other in solid phases, they differ in fluid phases since P/T remains close to its equilibrium value for sheared thermal ($T > 0$) fluids while $P \sim \dot{\gamma}$ at $T = 0$.